

GHz Ultrasound and Electrode Chip-Scale Arrays Stimulate and Influence Morphology of Human Neural Cells

Priya S. Balasubramanian and Amit Lal, Senior Member, IEEE

Abstract—This study describes the effects of chip-scale gigahertz (GHz) ultrasound (US) and electrical stimulus on the morphology, functionality, and viability of neural cells in vitro. The GHz frequency stimulation is achieved using aluminum nitride piezoelectric transducers fabricated on a silicon wafer, operating at 1.47 GHz, corresponding to the film's thickness mode resonance. These devices are used to stimulate SH-SY5Y neural cells in vitro and observe effects on the morphology and viability of the stimulated cells. It is possible to use these devices to deliver either ultrasonic stimulus alone or US stimulus in conjunction with electrical stimulus. Viability tests demonstrated that the neurons retained structural integrity and viability across a wide range of GHz US stimulus intensities (0-1.2 W/cm²), validating that measurements occur at nontoxic doses of US. Neural stimulation is validated with these devices following the outputs of a previous study, with the normalized fluorescence intensity of activated cells between 1.9 and 2.4. The 300-s ultrasonic stimulation at 1.47 GHz and 0.05 W/cm² peak intensity led to a decrease in nuclear elongation by 17.5% and a cross-sectional area decrease by 17.8% across three independent trials of over 150 cells per category (p < 0.01). The F-actin governed cellular elongation increased in length by up to 16.3% in cells exposed to an ultrasonic stimulus or costimulus (p < 0.01). Neurite length increased following ultrasonic stimulation compared with control by 75.8% (p < 0.01). This article demonstrates new GHz US and electrical chip-scale arrays with apparent effects in both neural excitation and cell morphology.

Index Terms—Gigahertz (GHz) ultrasound (US), neural stimulation, RF MEMS, ultrasonic bioeffects.

I. INTRODUCTION

GIGAHERTZ (GHz) ultrasound (US) has an immense potential to revolutionize the study of neurons using integrated chip-scale systems. Earlier research points to the use of this localized wavefront for the stimulation of neural cells at single-cell resolution [1], [2]. Theoretically, using the wavelength imposed resolution limit, 1.5-GHz US can reach 1- μ m lateral resolution in tissue with an attenuation profile localized wavefront to 10–20 μ m axially.

Manuscript received October 4, 2021; accepted February 13, 2022. Date of publication February 18, 2022; date of current version May 26, 2022. This work supported in part by the National Science Foundation under Grant 1744271 and in part by the Intelligence Advanced Research Projects Activity (I-ARPA) trusted integrated chips (TIC) Grant. (Corresponding author: Priya S. Balasubramanian.)

The authors are with the School of Electrical and Computer Engineering, Cornell University, Ithaca, NY 14853 USA (e-mail: psb79@cornell.edu).

Digital Object Identifier 10.1109/TUFFC.2022.3152427

This level of confinement has a high impact on the arena of single-cell engineering in chip-scale systems. Furthermore, the high-frequency GHz US stimulation is a novel mechanical stimulation approach with different temporal properties that could influence nuclear processes and larger scale cell mechanics through entirely different pathways.

Electrical and ultrasonic stimulation effects on ion channels and cellular differentiation have been studied extensively across different frequencies, intensities, and waveforms [1]-[10]. However, these effects have been described for ultrasonic and electrical stimulus systems administered as separate modalities and in independent studies [4]-[10]. There is a clear need for integrating these systems, especially since neural tissue is both electrically excitable and structurally sensitive to mechanical stimulus. The challenges to developing such a system are the design and interface of the chip and the stimulus to a single neuron or at least just a few neurons [2], [5], [8], [11]. Most US stimulation systems retain high penetration into tissue and induce stimulation and cellular effects; however, they are not able to reach the potential to engineer the neural tissue at the single-cell level. Ultrasonic stimulus in the kilohertz to megahertz frequency range has been widely used in both research and clinical applications to stimulate cells and tissue alike, with cited stimulation localization at 1 meter to tens of micrometers in spot size. Numerous studies highlight the potential of electrical and ultrasonic stimuli to stimulate, influence, and even differentiate neural cells.

Previous studies have uncovered various bioeffects due to ultrasonic and electrical chip-scale stimulation. In ultrasonics, stimulation waveforms have been primarily in the low-frequency to high-frequency bands with wavelengths much larger than neurons; thus, localization is often compromised. For chip-scale electrical stimulation, spatial localization requires high-density electrodes, and frequencies used are often below 100 Hz and usually at most in the kilohertz regime. Furthermore, these effects are thus far entirely investigated through systems that stimulate with either US or electrical stimulation separately.

There are a few critical studies in the area of ultrasonic stimulation to highlight. Lee *et al.* [12] use dual-frequency low-intensity US to stimulate attachment and differentiation of neural stem/progenitor cells. The primary resonance frequency of the transducer is 1138 kHz with a secondary resonant frequency of 560 kHz [12]. Lv *et al.* [13] use low-intensity pulsed US to stimulate proliferation and viability of induced

1525-8955 © 2022 IEEE. Personal use is permitted, but republication/redistribution requires IEEE permission. See https://www.ieee.org/publications/rights/index.html for more information.

pluripotent stem-cell-derived neural crest stem cells. The 1-MHz transducer is used with a pulse frequency of 100 Hz and induces upregulation of genes associated with differentiation [13]. In another example, Lee et al. [14] observe differentiation, enhanced neurite growth, and improved attachment of neural stem/progenitor cells under ultrasonic stimulation frequency of 1.8 MHz from 100 to 500 mW/cm² intensities. While cellular differentiation and regeneration might be desirable effects in clinical biodevices, ultrasonics may also induce cellular apoptosis. Balasubramanian [3] use 92-kHz ultrasonics and find that apoptosis is induced in the SH-SY5Y neural cell line past an intensity threshold. Tang et al. [11] use 1.75-MHz focused continuous US stimulation at an acoustic power of 1.4 W/cm² \pm 0.07 W/cm² for 3-min incident upon Sarcoma 180 cells and find that the mechanism of US-induced apoptosis could be NF- κB activation as an early stress response. Feng et al. [15] observe that 1.2-MHz US at 3.0 W/cm² for 1 min leads to induced early apoptosis. At the deoxyribonucleic acid (DNA) and chromatin morphology and effects level, Noriega et al. [16] observe chromatin condensation and increase in packing in L929 murine fibroblasts exposed to 5-MHz US at 14 kPa.

In the arena of electrical stimulation, various studies cite similar effects. Neural differentiation has been enhanced using multiple electrical stimulation techniques. For example, Guo et al. [17] demonstrated the differentiation of mesenchymal stem cells to a neural lineage using the conductive reduced graphene oxide (rGO)–poly (3,4-ethylenedioxythiophene) hybrid microfiber interface to stimulate cells with pulsed electrical stimulus using a triboelectric nanogenerator. The design is such that the scaffold may be self-powered by bodily movements to assist in neural regeneration applications [17]. While Yang et al. [18] decide to find the therapeutic range of electrical stimulation using a cell apoptosis assay, Kondo et al. [19] find that electrical stimulation may be potentially protective against apoptosis within a certain cellular environment. Thompson et al. [20] find that the neurite outgrowth is enhanced with 250-Hz biphasic, 100- μ s pulsed, ± 1 -mA/cm² electrical stimulation, which works synergistically with neurotrophins to promote neurite growth. A supporting study by Evans et al. [21] finds that electrical stimulation through coated electrodes is synergistic in promoting neurite outgrowth in spiral ganglion neuron explants. Electrode array designs presented in various studies attempt to localize stimulus and sensing using high-density electrodes, one example having a $20-\mu m$ electrode separation [22].

In chip-scale neural systems, previous literature highlights various bioeffects of electrical and ultrasonic stimulation separately. To date, there are no devices that have intended costimulatory actions with both electrical and ultrasonic stimulation in the GHz regime. This type of stimulus can be seen as biomimetic. This is because in true biological systems like the developing and mature central and peripheral nervous systems, localized electrical and mechanical stimuli are naturally occurring and drive various critical processes. As such, chip-scale neural systems will be most successful at producing intended biological effects if they can produce both mechanical and

electrical stimuli. Thus, both the costimulus and the highly localizable GHz wavefront are novel claims of this study and the presented devices. This study introduces system design parameters that allow for understanding how highly localizable GHz-US costimulation might influence cellular characteristics in neural systems, including cell health, differentiation, morphology, and stimulation of ion channels. The following results use the well-known frequency dependency of minimum focal spot size to further push neural engineering limits at the GHz regime in an SH-SY5Y human neural cell system.

This article presents three renditions of the GHz US and electrical chip-scale array-based waveform delivery with three modes of operation possible: 1) GHz frequency US stimulation; 2) GHz frequency US and electrical costimulation; and 3) GHz US and decoupled, direct electrical stimulation. These modes of operation are described in Fig. 1. Stimulation A is achieved with the transducer on the bottom, isolated from neurons by the silicon wafer bulk, and can only excite the cells using GHz US. Stimulations B and C are accomplished by the additional electrodes on the interface directly near the cells that can be sonically or directly stimulated to create electrical fields, which are applied in conjunction with bottom-side GHz US transducer activation. Device C electrodes are driven with 50-Hz stimulus and 500-mV peak drive voltage with square wave input as per previous neural cell culture system stimulation protocols.

The integration of ultrasonic transducers with tissue-compatible electrodes is novel to the landscape of neural interface devices, with significant implications for many fields ranging from cellular engineering to medical prosthetics. This study is the first study to quantify morphologic change to a neural cell undergoing differentiation under the stimulus of GHz US and the first article to report the intended use of GHz ultrasonic and electrical costimulus.

II. METHODS

Transducers used in this articles experimental section are described that pertain to each of the three types of devices used in this article in Fig. 1. These transducers were designed in batch as a part of a process flow to develop one of the first chip-scale GHz ultrasonic arrays, used in a wide variety of applications, including but not limited to neural stimulation, imaging of fingerprints, and thermal monitoring [23]. Various studies have developed single-element GHz US transducers or GHz ultrasonics for acoustic microscopy applications [24], [25], however, these chip-scale GHz ultrasonic transducers are the first to be designed for neural stimulation specifically and are a part of a group tape-out. To meet the needs of the applications they are designed for, the transducers are designed to operate within the 1-2-GHz range, novel in the field of chip-scale ultrasonics due to the high operating frequency and chip-scale arraybased format. These transducers use a thin-film aluminum nitride (AlN) deposition that allows for operating resonance range with a center bandwidth at 1.47 GHz. This chosen operating frequency not only allows for a theoretical micrometerlevel localization in aqueous medium but also is the center bandwidth resonance of these devices, fabricated in collab-

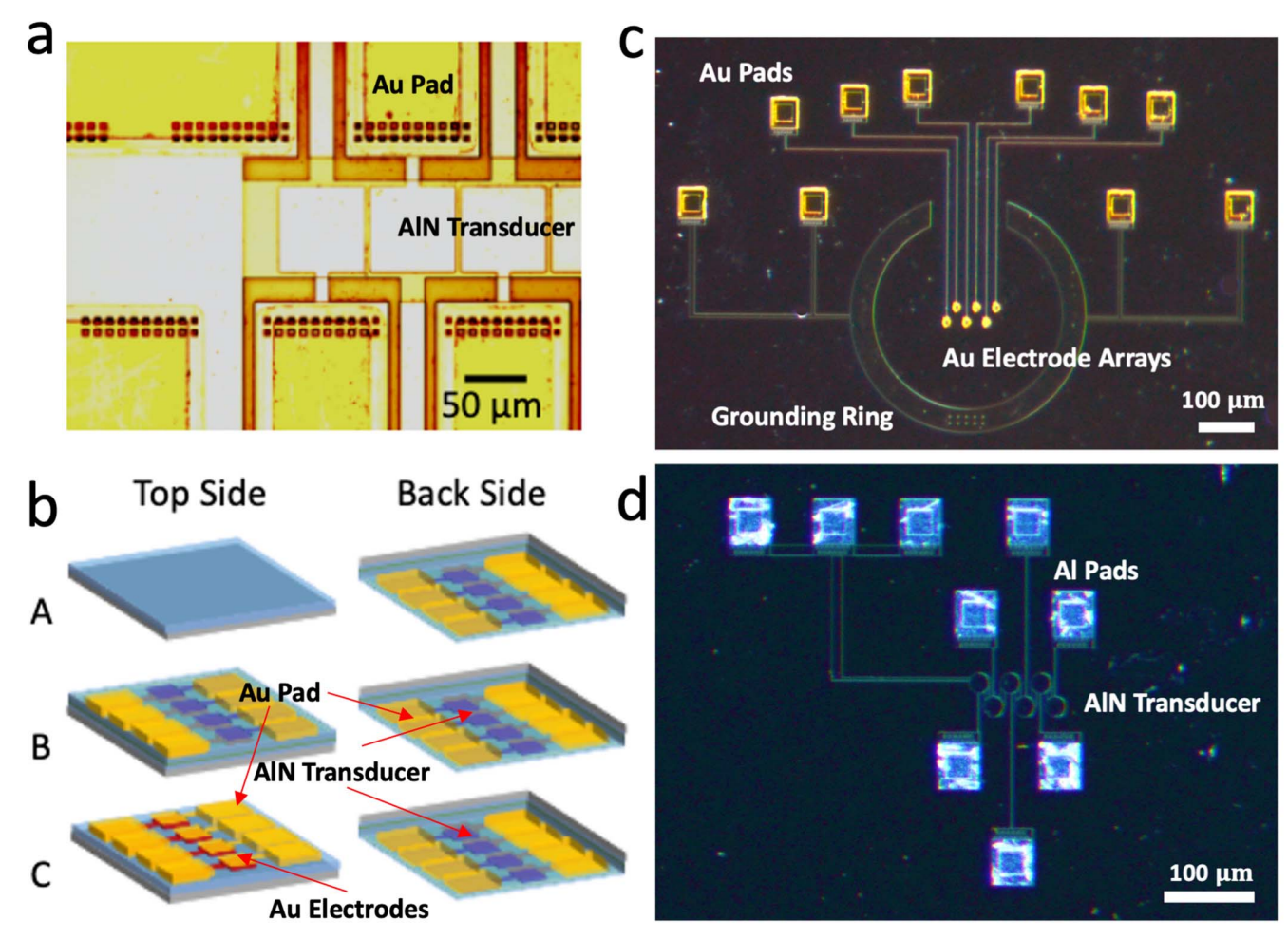


Fig. 1. (a) Light microscopy image of ultrasound transducers and gold electrode pads in Devices A and B. (b) All three chip layouts used in the study, labeled Devices A, B, and C. Backside of all devices contain AlN ultrasound transducers. The top side, interfaced to neurons, has no devices (A), AlN transducers (B), and gold electrodes (C). Interface with cell culture schematics shown in Fig. 4(a). (c) Brightfield image of Device C top side with Au electrode arrays and grounding ring structure. (d) Brightfield image of Device C bottom side with electrode arrays and Al contact pads.

oration with Institute of Microelectronic (IME) Agency for Science, Technology and Research (A*STAR), Singapore, as a first in the field of ultrahigh-frequency ultrasonics for neural stimulation. Furthermore, high-frequency ultrasonics will be more attenuating, and the $10-20-\mu m$ axial localization of the 1.47-GHz ultrasonics is ideal for a biological application as small volumes can be targeted, and dosage reduced to further localize axially. Higher attenuation profiles lead to the risk of localization restricted to the chip surface, which is not ideal for medical applications. The three device types presented have unique functionalities. Device fabrication of transducers is performed at IME A*STAR, Singapore, and the layout is shown in Fig. 2. The transducers' preparation and interfacing with electronics and RF sources is performed through an RF-compatible two-sided PCB, which allows for wire-bonding to both the bottom and topside transducer and electrode devices. Device A (electrode-free surface) has AlN US transducers fabricated on the backside of the chip with Au contact pads. Device B (GHz costimulatory) has these identical transducers manufactured on both sides of the chip. Device C has AIN US transducers fabricated on the backside of the chip with Al contact pads and Au contact electrodes fabricated on the interface or top side of the chip. Devices B and C are

capable of costimulation with both electrical and ultrasonic stimuli, either with US -induced electrical stimulation at GHz frequency or decoupled waveform input. Fig. 5 depicts the US intensity measurements and electrical field measurements as described in further parts of Section II.

The cell culture protocol used in this article follows closely what was used in [1], [26], and [27]. SH-SY5Y neuroblastoma cells were seeded at 15 000 cells/cm² onto glass coverslips. After 48 h of growth, a final cell surface density was observed at 50%–70% cell confluency. Subsequently, these cells were differentiated to push from epithelial to neural phenotype for another 48 h. The glass slide with seeded and growing cells was brought in proximity with the ultrasonic transducer chip with a gap of 10–15 μ m between the transducer and the sample coverslip using 10 μ L of cell media. The supplemental section describes staining protocols for transient ion imaging, cell viability characterization, and nuclear and F-actin staining.

A. Transducer Process Flow

The devices used in the article have process flows with resultant layers as depicted in Fig. 2. Device A is depicted in Fig. 2(a), Device B is described in Fig. 2(b), and Device C

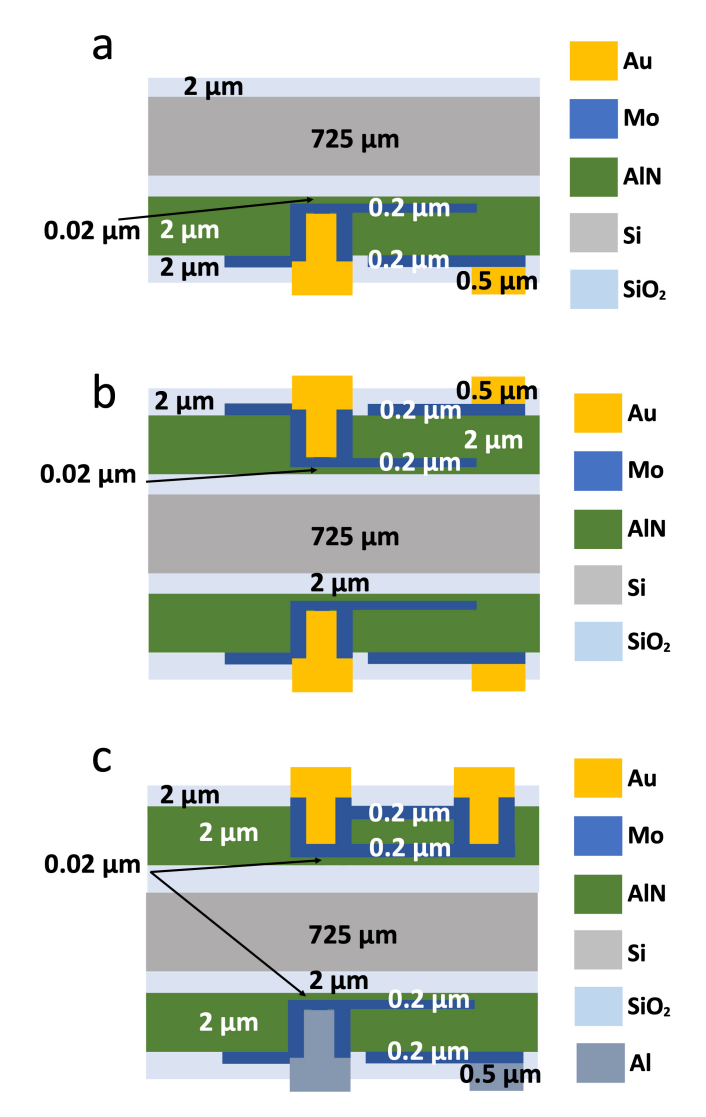


Fig. 2. (a) Process flow layer stack for Device A, which is a one-sided ultrasound transducer chip with a center resonance bandwidth of approximately 1.47 GHz. (b) Process flow layer stack for Device B, which is a two-sided identically fabricated ultrasound transducer chip, which can costimulate cells with electrical stimulation on the top surface due to exposed gold pads at the same resonance as the ultrasound transducer operation. The thin-film AIN has a center resonance bandwidth of approximately 1.47 GHz. (c) Process flow layer stack for Device C, which is a two-sided process flow with gold pad electrode arrays on the top interface surface and aluminum pads on the ultrasound transducer surface. The ultrasound transducers have a center resonance bandwidth of approximately 1.47 GHz. AIN and SiO₂ are used as insulators for the electrode array on the top surface.

is shown in Fig. 2(c). All the devices feature gold electrode pads at least on the surface, with Device C using aluminum contact pads for transducers on the noninterface surface, but bio-compatible gold electrodes on the cell interface surface. The US capacity of the devices is realized through thin-film AlN deposition, with a $2-\mu m$ layer corresponding to a center bandwidth of the resonance at 1.47 GHz, used in the remainder of this study. The chip shots of the devices are shown in Fig. 3, and individual devices are shown in Fig. 1.

The fabrication of these devices used the following core process flow for one side of the wafer. Two-sided devices follow the same process flow for both sides of the wafer.

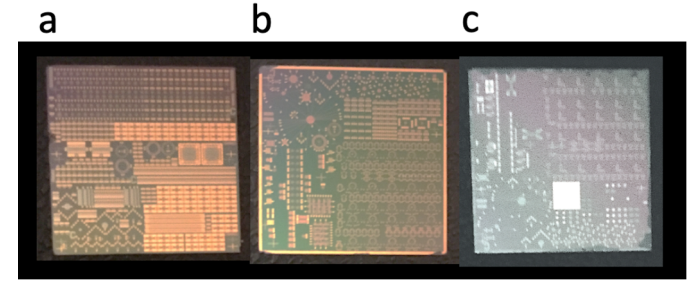


Fig. 3. (a) Chip shot of Device A and Device B, with Device B having an identically fabricated bottom surface, approximately $2 \text{ cm} \times 2 \text{ cm}$ in size. (b) Chip shot of Device C electrode array side with gold contact pads. (c) Chip shot of Device C ultrasound transducer array side, with aluminum contact pads.

The 2- μ m SiO $_2$ was deposited using plasma enhanced chemical vapor deposition (PECVD) on the surface of the 725- μ m silicon wafer. Following this, a seed layer of AlN was deposited at a thickness of 20 nm with physical vapor deposition (PVD) through magnetron sputtering. The bottom molybdenum electrode was similarly deposited through PVD at a thickness of 0.2 μ m. The bottom Mo electrodes were patterned using reactive ion etching. Following this, the 2- μ m AlN was deposited, and the top electrode Mo was also deposited and patterned using reactive ion etching. Vias were created to connect the top and bottom Mo layers through hot phosphoric acid etch of AlN. Gold (Au) or aluminum (Al) was deposited through PVD by sputtering and pattered through etching. SiO $_2$ was deposited at a 2- μ m thickness through PECVD, and contact pads were exposed through reactive ion etching.

As shown in Fig. 3(a), the approximately 2 cm \times 2 cm chip of Device A and Device B layout has an array of ultrasonic transducers, one of which was used in the experiments in Sections III-A–III-D. A 70- μ m square transducer was chosen and wire-bonded at the bottom side of the chip-scale device, and the top interface side of the chip interface with cells was imaged directly above the active transducer, in the area of the far-field diffraction pattern. The transducer used is additionally shown in Fig. 1(a).

As shown in Fig. 3(b), the top side of Device C is visible, which is designed with circular gold electrodes of varying diameters (devices may have 10, 20, or 40 μ m electrodes), with a grounding ring structure, as shown in Fig. 1(c). These devices use high-density and small-sized contact pad electrodes in array format. As shown in Fig. 3(c), the device's backside has circular US transducers at the same operating resonance as Devices A and B, which are in array format as shown in Fig. 1(d). It can be either 40 or 80 μ m in diameter. For the data depicted in this article, 10- μ m electrodes in array format similar to Fig. 1(c) were used with a grounding ring structure and 20- μ m center-to-center electrode pitch, with a bottom side 40- μ m diameter US transducer array with a 50- μ m center-to-center pitch similar to Fig. 1(d).

B. Device Interface and Properties

The *in vitro* cell interface layout and optical interface for each device type in addition to the electric field localizations

are shown in Fig. 4. Devices B and C have electric fields that are sonically activated and independently controlled through electrode arrays, respectively. The interface for Device C is distinct due to the surface wire bonds, as shown in Fig. 4(a). The details of the device interface as depicted in Fig. 4(a) are described extensively in Balasubramanian et al. [1], [2] Cells were grown on glass coverslips, as described in detail in methods in Section II-D of this article, and then inverted and placed 10 μ m away from the surface of the chip-scale device using a controlled volume of cell culture medium. This method was reproduced exactly from the supporting previously published research [1], [2]. The device resonance and electrical field properties for Device B were characterized using a 10-GSamples/s RTO 1024 oscilloscope and verified using a Polytec UHF interferometer. Measurements consisted of averaging at least ten complex-valued acquisitions during continuous wave excitation of a 70-µm transducer. The farfield diffraction pattern displacement data are depicted in Fig. 5(c) at the opposing surface of the activated transducer. For Device B, the voltage across the top gold pads was 25 mV_{pp} as a result of the sonically activated electrodes during ultrasonic stimulation at 0.05 W/cm², as shown in Fig. 5(a). Fig. 5(b) depicts an extrapolation of displacements using the obtained linear correlation between displacement and voltage from a previous research [1], and Fig. 5(c) provides the farfield diffraction pattern. Device C has decoupled electrodes as shown in Fig. 4(c), which were driven with 50-Hz stimulus and 500-mV peak drive voltage with square wave input.

C. GHz US Effects on Action Potentials

To observe ion channel stimulation, a minimum of 10 s of prestimulus data was obtained. For Devices A and B, 20 s of continuous wave GHz ultrasonic stimulation was applied following the initial prestimulus. Post stimulation, ionic transients were recorded for a total of 50 s, giving a total recording time of 80 s. For Device C, 30 s of electrical stimulation was applied, followed with 30 s of costimulation with GHz US. Data were collected on n > 50 cells per condition. To provide negative controls for neural stimulation, both off-resonance drive voltages and gentamicin treatment with 2-V, 0.05-W/cm² stimulus drive were applied. The off-resonance frequency input was provided at 300 MHz at $2V_{\text{peak}}$ on to the backside transducers. This should neither induce ultrasonic stimulus nor electrical stimulation. It gives a valid control for decoupling potential through silicon electrical stimulation. Gentamicin is a calcium ion channel blocker and was administered following standard protocols, and it was loaded at 200 mM in Hank's Buffered Saline Solution (HBSS) for 60 min at 5% CO₂ and 37 °C. This control decouples potential secondary effects causing ionic flux (such as membrane sonoporation). Fluo-8 AM calcium chelator was loaded for calcium flux acquisition to image the action potential of cells. The protocols follow exactly previous research in the laboratory. The image frame rate was set to upward of 20 frames/s. Time point analysis was performed following image processing algorithms outlined in Section II of prior publications and other supporting research [1], [2], [28], [29]. Data were quantified as time point averages in bar graph format. The regions of interest (ROIs)

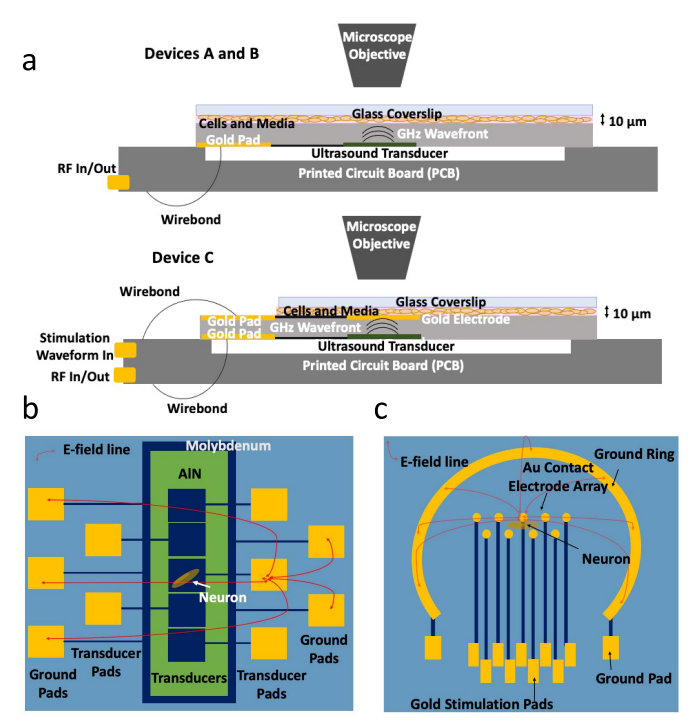


Fig. 4. (a) Schematic of device interface with neural cells cultured on glass coverslips for Devices A and B on the top and Device C on the bottom. (b) Example electric field lines for Device B top-side costimulatory ultrasonically activated and coupled electrode array. (c) Example electric field lines for Device C which has top-side decoupled electrodes in gold, featuring a high-density, small-sized array format for these electrodes and a grounding ring structure.

were obtained using the previous research's segmentation and region identification algorithms [1], [2], [28], [29]. ROIs were obtained in a semiautomated manner, through threshold-based segmentation of the image, and visual and manual identification verification by an experienced biologist following automated segmentation. Each ROI approximates a cell, 20 μ m \times 20 μ m in size within the cell culture interface. To analyze the data, data were normalized by subtracting a background region of 50 \times 50 pixels (F_b). This region has little to no relevant calcium transient signal. All fluorescence intensity (FI) levels were scaled to the pixel-by-pixel average of the initial 5 s of data which is called F_o , which is prestimulus. F_i designates these initial time points of data. The value F_o was thus defined as $F_o = \sum_{t=0-5s} (F_i - F_b)$. Following this, the FI was normalized at each time point to depict the calcium transient activity. The normalized FI was computed as follows: $(F_t - F_b)/(F_o)$, where F_t is the FI at any time point t. A 0.5-s moving averaging window was used to reduce noise in the time course data analysis. Trials were classified as activated by ultrasonic and/or electrical stimulus if two criteria are met. First, there must be a statistically significant difference in F_t between the prestimulus (5 s) and poststimulus (70 s for Devices A and B and 50 s for Device C) time points at an alpha level of $\alpha = 0.01$. Second, there must be visible calcium transients, indicating action potentials, in the time course data following but not preceding the stimulus. This analysis is supported by previous research published by Balasubramanian et al. [1], [2], and the technique toward analysis is supported by cited literature [28], [29].

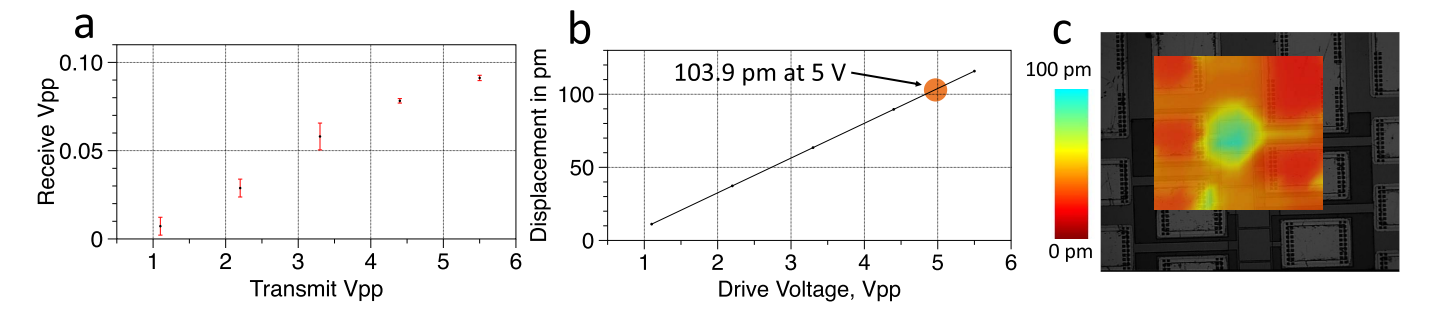


Fig. 5. (a) For Device B, the top-side transducers are ultrasonically activated by the bottom-side transducers. Once an RF input is applied to the bottom-side transducers, an ultrasonic wave is generated when RF input is supplied at resonance, and this ultrasound wave traverses through the silicon chip and interacts with the identically fabricated top-side transducer, which causes an RF electric field on the surface of the chip. This plot shows the input voltage of the transmit transducer and the related receive voltage of the top side identically fabricated transducer. (b) From previous work, a linear correlation is observed between displacement and input drive voltage. The displacement of the transducer across voltages is extrapolated from a datapoint obtained with the maximum displacement across the spatial profile under a 5-V drive input. (c) Spatial displacement profile of the far-field diffraction pattern with a 5-V input drive voltage on a bottom-side transducer in Device B.

D. GHz US Effects on Cellular Morphology Using Chromatin and F-Actin Staining

An analysis of the morphological effects of GHz ultrasonics was performed through characterization of F-actin and nuclear morphology. F-actin was stained using a phalloidin conjugate with fluorescein isothiocyanate (FITC) excitation emission ranged, and thus imaging was performed on a broadband source microscope with an FITC filtering system. Nuclear morphology was characterized through 4' 6, diamidinophenylindole (DAPI) staining. Representative staining images are shown in the associated figures of the main text. The characteristics of the DAPI-stained nuclei and phalloidinstained F-actin were analyzed through quantifications using the open source Image J National Institutes of Health (NIH) tool kit. The outputs include nuclear shape and size and F-actin major axis and neurite length. The effects were analyzed on a set of images for at least three repeated trials of stimulation for 300 s under the acoustic field of one ultrasonic transducer in the field of view of the image.

The cells were grown for a total of 48 h on a glass coverslip in Eagle's minimum essential medium (EMEM), serum supplemented medium to achieve 50%-60% confluency. The cells were grown for another 24 h in EMEM, partially serumdeprived medium, supplemented with retinoic acid (RA) to induce differentiation that resulted in a confluency closer to 60%-70% and neurite outgrowth. Following this, cells were exposed to US stimulus by interfacing the prepared glass coverslip (22 mm × 22 mm) directly with the ultrasonic transducer 10 μ m away from the transducer surface. Cells were stimulated with US for 300 s, and then the coverslip was infiltrated with 250 µL of medium to detach it from the transducers. The coverslip was lifted off the transducer chip directly perpendicularly to the surface of the chip, as to avoid causing shear stresses. The cells were reloaded with 100 μ L of medium and placed back in the incubator at 37 °C and 5% CO₂ for another 24 h. Cells that were not stimulated with ultrasonics and serve as a control were still interfaced with the transducer for 300 s. This is important because the shear stresses and other external factors that may influence the cells during the interface process that are unrelated to US must be ruled out as factors influencing the morphology and characteristics

of the cells. After 24-h poststimulus cell growth in retinoic acid supplemented, partially serum deprived medium, cells were prepared for staining. The medium was aspirated, and cells were washed three times in phosphate-buffered saline (PBS). Following this, cells are placed in 4% formaldehyde in PBS, with 250 μ L placed per glass coverslip, and incubated for 30 min. Subsequently, cells were rinsed three times with PBS. Afterward, cells were stained with imaging agents, first with phalloidin, and then subsequently with DAPI, following recommended diluting agents, temperature conditions, and loading concentrations. Each incubation was performed for 30 min consecutively, and the protocols provided by reagent manufacturers were followed for the staining and conjugate storage protocols. Microscopy techniques and instruments were similar to those used in previous studies and preceding methods, with exposure times optimized to ensure proper signal acquisition. Exposure and imaging were performed under identical settings per stain type. In addition, background signal was removed as a postprocessing step and images were standardly processed to obtain comparable contrast for quantification to yield accurate results. For intensity measurement quantifications, only background signal removal was performed without any contrast enhancement as the intensity should be post background signal removal to obtain accurate results. The processing was performed on ImageJ software (NIH); however, all the measurements were drawn in a nonautomated manner, and ImageJ was used to compile the lengths of the measurement marks. The measurements for neurite length, cell major axis length, nuclear aspect ratio, and nuclear area are all performed by an experienced biologist with expertise in neural cell culture. These experiments were performed three times each for Devices A and B and for a no US control. Device C was excluded from this section due to wire-bonding intricacies that make removal of cells challenging until chips are integrated. Images were quantified and analyzed on ImageJ and MATLAB MathWorks 2019a.

E. Cell Viability Under GHz Ultrasonics Stimulation

Section III outlines toxicity studies to ensure that the costimulus is nontoxic to cells. To evaluate this, Caspase-3 and Annexin V staining agents were used to evaluate for

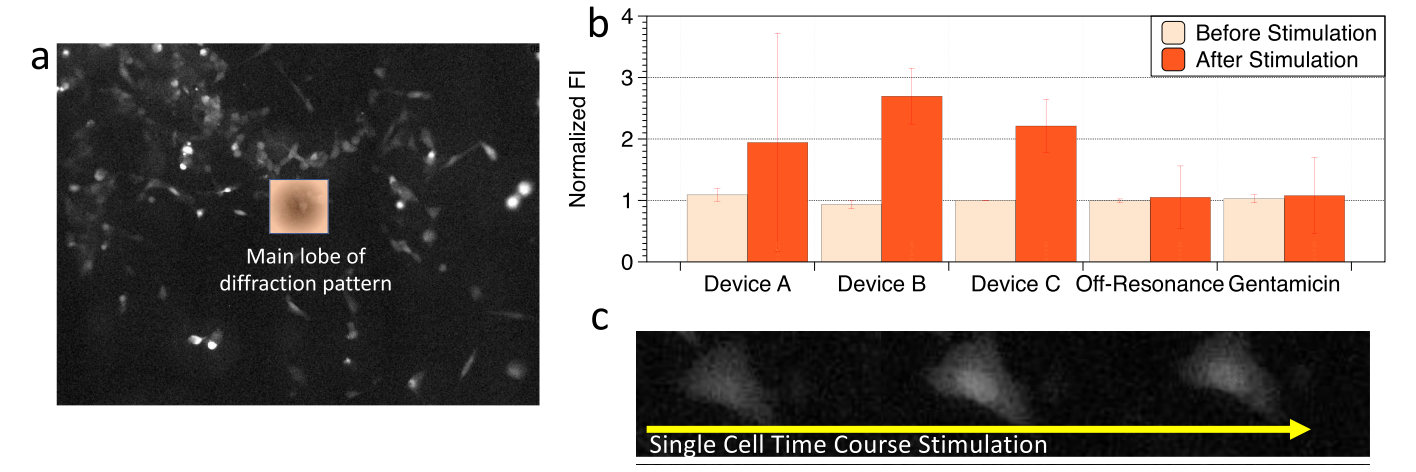


Fig. 6. (a) Field of view of the calcium imaging data acquisition and the main far-field diffracting lobe of the ultrasonic wavefront is shown for a single frame of the time course stimulation data, which has a 10-s prestimulus period, 20-s stimulus, and at least 60 s of poststimulus recording for Devices A and B, and prestimulus data of 10 s are collected for Device C, and following this, 30 s of electrical stimulation is administered at 50 Hz, 500 mV peak, square waveform, following costimulation with both ultrasonic and electrical stimulation with a 0.05-W/cm² ultrasound stimulation intensity. (b) Time point activation (50 s for Device C and 70 s for all other devices) compared with resting state at t = 5 s. Significant (p < 0.01) activation was observed for all three device types when comparing normalized stimulation intensity before and after stimulation for each device type and observing a statistically significant difference, with no activation for negative controls. (c) This subfigure shows one example time course stimulation of a cell at three different time points with ultrasound stimulation, with time increasing following the arrow. Calcium transients can be visualized as increases in FI over time, and the middle time point has the strongest signal in this subfigure, indicating a calcium flux.

potential apoptosis and Calcein-Blue AM loading for membrane integrity and cell health. In addition, Fluo-8 AM loading was used to determine the pre- and poststimulus viability changes from a range of 0-1.2 W/cm². Intensity changes were calculated through the following normalized FI equation, $(F_{\text{final}} - F_{\text{background}})/(F_{\text{initial}} - F_{\text{background}})$, where F_{final} was the FI at a time point following stimulus, and F_{initial} was the FI at a time point preceding stimulus and the background was a part of the field of view containing signal that was predominantly not temporally varying due to the changes in the cell. The ultrasonic intensity was applied for 20 s in this experimental protocol and tested 120 s after exposure, during substantial action potential activity decrease. The background signal was removed to compensate for photobleaching effects. Calcein-Blue AM (excitation/emission characteristics following DAPI filtration cube parameters) was loaded into the cells after 24 h of growth following the 300-s exposure as outlined in Section II-D. Quantification was performed in a similar manner to Fluo-8 AM characterization. Caspase-3 and Annexin V staining was performed following 300 s of ultrasonic stimulus and 1 h of incubation with costimulatory GHz Device B, kilohertz resonance transducers at high intensity (92-kHz resonance, piezoelectric ceramic 22-mm disk) and a healthy control. The kilohertz transducer treatment at an intensity >5 W/cm² acts as a positive control. At least three repeated trials and subsequent staining were evaluated for each condition.

III. RESULTS

A. GHz Chips Stimulate Ion Channels

Fig. 6(a) shows an example frame of the video data acquired for stimulation analysis. Fig. 6(b) shows the ROI analysis before and after stimulus select time points, supporting previous work [1], [2]. Fig. 6(c) shows one select cell across

time that is stimulated by GHz US. The relevant negative controls (off-resonance and gentamicin) are provided. Each device type demonstrated statistically significant stimulation compared with the resting state at an alpha level of 0.01 with normalized FIs reported at >1.4. This provides proof that each type of device outlined can be used in ion channel stimulation.

B. GHz Ultrasonic Stimulus Leads to Circular Nuclear Morphology and Chromatin Condensation

The influence of GHz ultrasonic stimulation on nuclear morphology was investigated. The cross-sectional area of the cell nucleus and the nuclear elongation factor was optically imaged. These measurands provide cues into chromatin condensation and the overall structural information of the cells and forces exerted on the cell's nucleus. Devices A, B, and US-free control are compared. The results show that for a population of cells from three separate trials for each subcategory, with at least 150 cells analyzed for each separate criterion (no US exposure, GHz costimulation, and one-sided devices), chromatin condensation and smaller and more spherical nuclei were observed when US is applied. A statistically significant difference is noted at an alpha level of 0.01 for all three devices, showing significant differences between costimulatory and electrode-free surface devices as well as compared with the US-free control data. A decrease in the nuclear aspect ratio of 17.5% and a cross-sectional area decrease of 17.8% were noted across three independent trials of over 150 cells per category (p < 0.01) [Fig. 7(a) and (b) with representative images in Fig. 7(c)]. In the comparison between costimulatory system and one-sided devices, the costimulatory system had less condensed chromatin and a larger aspect ratio of the nucleus and a more extensive range for both quantities (mean crosssectional area of 339.5, 295.1, and 383.7 μ m² and mean aspect

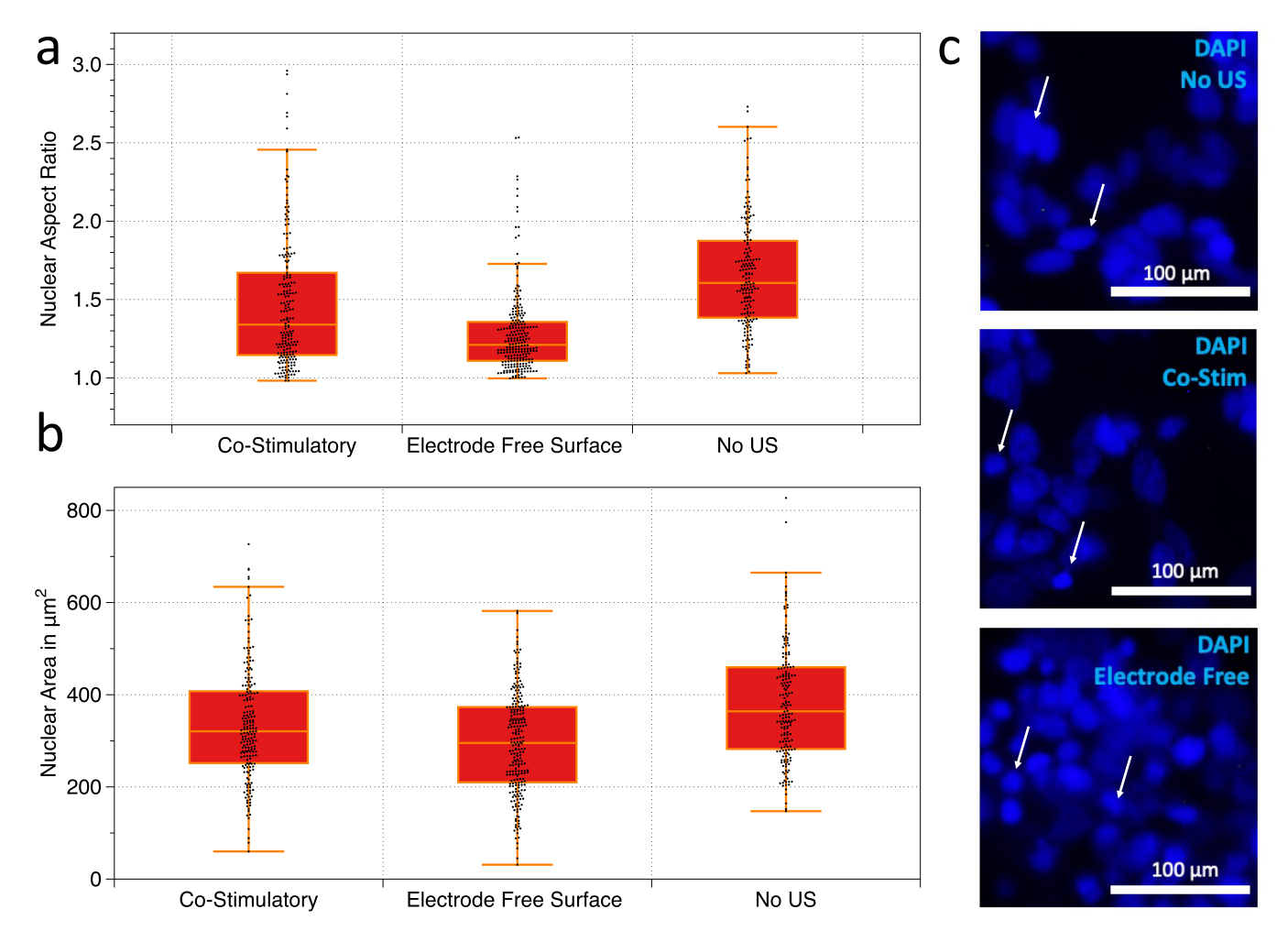


Fig. 7. (a) Nuclear aspect ratio shown with each data point depicted in box and whisker plot format for Devices A, B, and US-free control. Device A is labeled as electrode-free surface and Device B is labeled as costimulatory. (b) Nuclear cross-sectional area shown with each data point depicted in box and whisker plot format for Devices A, B, and US-free control. Device A is labeled as electrode-free surface and Device B is labeled as costimulatory. (c) Representative images of DAPI-stained nuclei for each condition. Device A is labeled as electrode-free surface and Device B is labeled as costimulatory. Device A and Device B show substantial compacting of chromatin and condensation as a result of ultrasonic and electrical costimulation. Data are obtained at the 24-h time point following stimulation for a 5-min period and standard cell culture incubation.

ratio of 1.47, 1.28, and 1.66 for costimulatory, electrode-free surface, and no US control devices, respectively).

C. GHz Ultrasonic Stimulus Leads to Cellular and Neurite Elongation

The differences in cell body elongation axis and neurite lengths of F-actin-stained cells were tested and significant among Devices A, B, and US-free control at an alpha of 0.05. Over 150 cells across three separate trials were analyzed for each device testing subset. Despite the nuclear and chromatin condensation reported in Section III-B, the major growth axis length of the cells was longer on average for the ultrasonic stimulus conditions. There was a 16.3% increase in cell elongation axis length when compared with no US control samples with 88.5-, 84.9-, and 74.1- μ m major axis length for costimulatory, electrode-free surface, and no US control devices, respectively. It is expected that electrical and ultrasonic stimulation will cause neurite extensions. Costimulus could result in better tunability due to the coupled effect when compared with the electrode-free surface devices [30]–[33]. The neurite length

increase was statistically more significant for Devices A and B than the US-free control, with a 75.8% increase compared with the US-free control, and average lengths of 44.8, 46.3, and 25.8 μ m for costimulatory, electrode-free surface, and no US control devices, respectively. The results are shown graphically in Fig. 8(a) and (b), with representative images in Fig. 8(c).

D. GHz US Is Nontoxic From 0 to 1.2 W/cm²

Fig. 9(a) provides negative apoptosis and necrosis staining results for GHz stimulation with positive and negative controls, as outlined in the supplemental methods' section. Fig. 9(b) shows no loss in calcium intensity across intensities of US stimulation for Fluo-8AM loading, further verified with unshown Calcein-Blue AM loading. It can be concluded that using traditional cell viability assays, GHz ultrasonic stimulation is nontoxic up to intensities of 1.2 W/cm².

IV. DISCUSSION

The findings of this article have substantial implications that ultrahigh-frequency RF band in both ultrasonic and

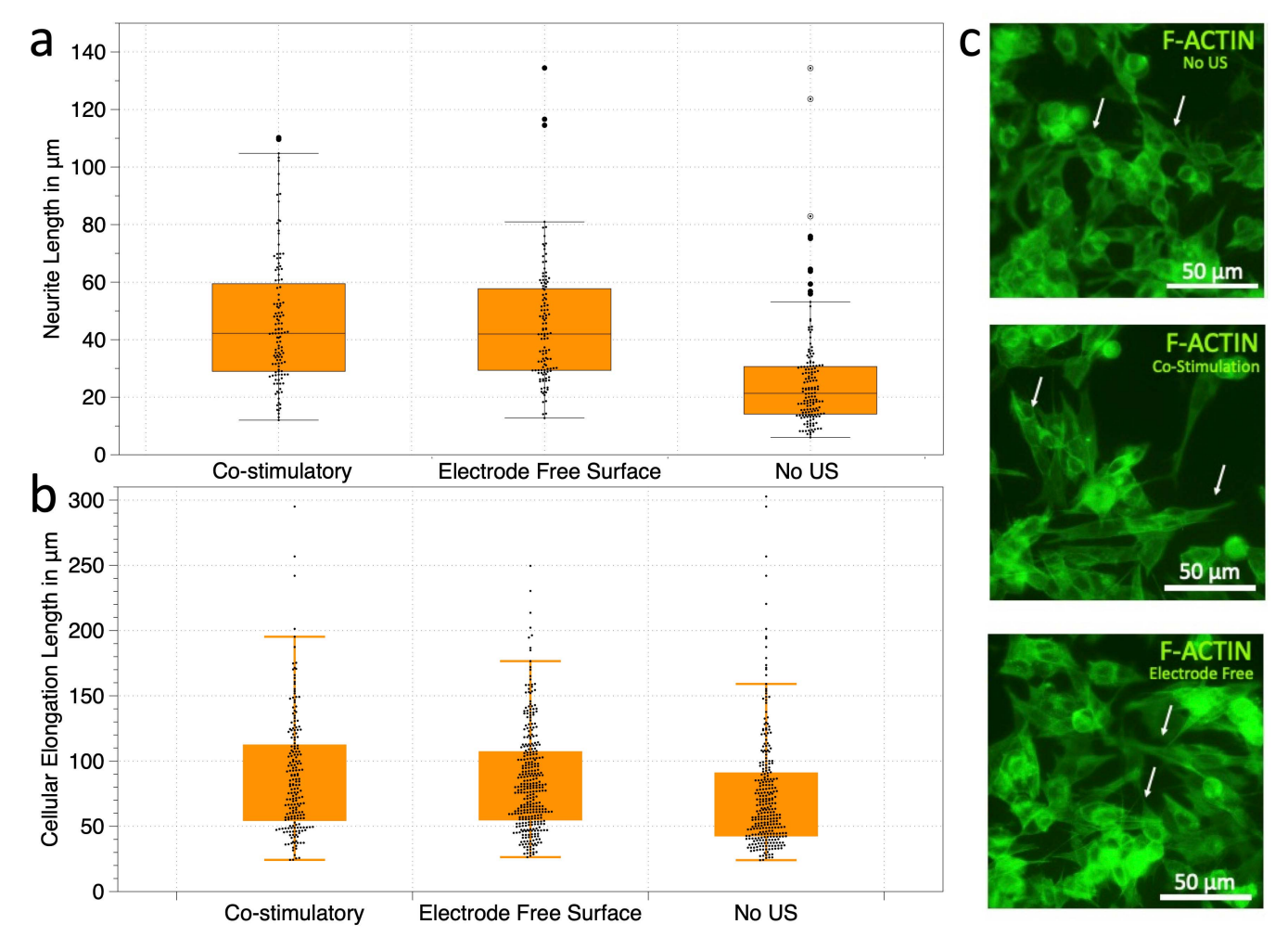


Fig. 8. (a) Neurite length in micrometers shown with each data point depicted in box and whisker plot format for Devices A, B, and US-free control. Device A is labeled as electrode-free surface and Device B is labeled as costimulatory. Neurite length quantification is enabled through F-actin staining with phalloidin. (b) Cellular elongation length (length of the main axis of the cell, or longest axis) in micrometers shown with each data point depicted in box and whisker plot format for Devices A, B, and US-free control. Device A is labeled as electrode-free surface and Device B is labeled as costimulatory. (c) Representative images of phalloidin-stained F-actin filaments for each condition. Device A is labeled as electrode-free surface and Device B is labeled as costimulatory. Device A and Device B show substantial compacting of chromatin and condensation as a result of ultrasonic and ultrasonic and electrical costimulation. Data are obtained at the 24-h time point following stimulation for a 5-min period and standard cell culture incubation.

electrical modes can influence the function and morphology and underlying features of human neural cells. There have been various attempts in the literature, as discussed in the introduction, to illuminate the precise influence of ultrasonic and electrical stimulus separately on neural cells in terms of stimulation of ion channels [1], [6], [9], [34]-[37] and various cellular bioeffects including neurite outgrowth, chromatin level changes, and apoptosis induction or prevention [3], [12], [16], [18], [19], [32], [14], [38], [39]. Most of these studies are focused on lower frequency bands, due to the challenges of highly attenuating ultrahigh-frequency ultrasonic wavefronts. Furthermore, electrical stimuli have traditionally been used at frequencies similar to naturally occurring biological stimuli. The attenuation properties of RF electrical fields at ultrahigh frequency also scale with the frequency, and thus, attenuation is enhanced, as is spatial localization. Resultantly, the devices presented in this study have enhanced localization using ultrahigh frequencies in both ultrasonic and electrical stimulation. Furthermore, Device B can

operate electrode arrays for stimulation without direct electrical connections, using silicon ultrasonic vias that communicate the generated US signal from the bottom-side transducers to the gold electrode pads of the identically fabricated top-side US transducers. Device C has decoupled electrode arrays that can be driven through surface wire bonds at any stimulation frequency with chosen stimuli closely following commonly used electrical stimulation protocols for ion channel stimulation. Thus, each of these devices presents an interesting contribution to the neural interface field. Device A proposes highly localization GHz ultrasonic interrogation of neurons, Device B proposes highly localized GHz ultrasonic and electrical coupled costimulation of neurons, and Device C proposes decoupled electrical and GHz ultrasonic stimulation.

The principle of these neural interfaces is to influence neurons in a localized manner with ultrasonic and electrical stimulation of the ultrahigh-frequency band. Previous studies illustrate that the ultrasonic dose (intensity) affects the stimulation of ion channels in a threshold-dependent manner for

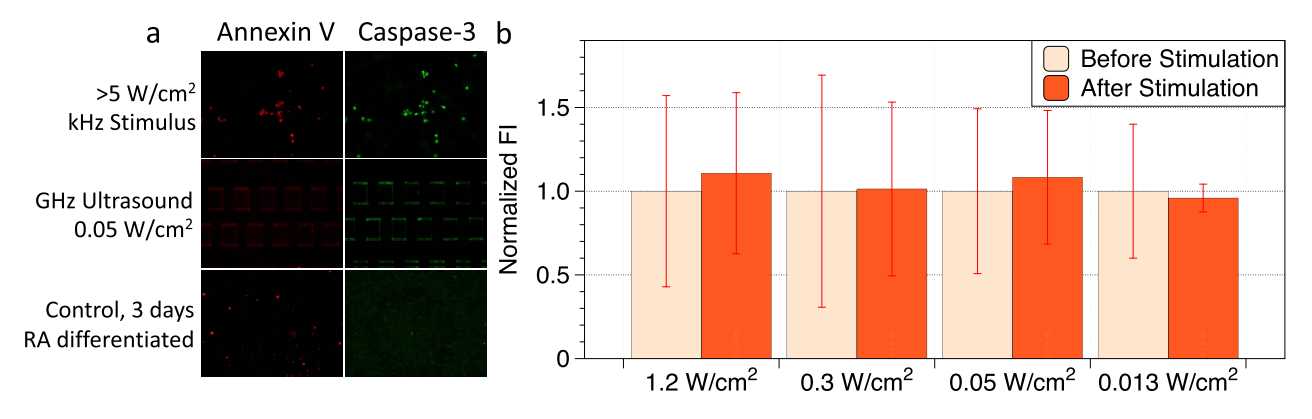


Fig. 9. (a) Low-level apoptosis and necrosis detected with GHz ultrasound at the intensity and frequency used in the remaining of the data figures in this article, comparable to negative US-free control, with positive apoptotic and necrotic markers shown for high-intensity kilohertz ultrasound stimulation of neurons in identical culture conditions. (b) Calcium loading indicates no toxicity and membrane damage across wide range of intensities of GHz transducers.

GHz ultrasonic stimulus [1]. Furthermore, Fig. 9 of this study illustrates that cell health and apoptotic markers are influenced by ultrasonic dose, and higher doses may negatively influence cell health. Thus, the performance of stimulation and cellular morphological change is influenced by dose. However, this study contributes one further observation that the utilization of costimulation with electrical and ultrasonic stimulation has a statistically significant influence on the system performance. This is evident in Fig. 7, where chromatin compaction and condensation are increased in Device A when compared with Device B, indicating that the electrical stimulus has an opposing influence on the chromatin. Following this, while both Devices A and B stimulate neurite outgrowth compared with US-free control group neurons, it is possible that the costimulatory Device B further stimulates neurite outgrowth and cellular elongation, as suggested by other studies that find that electrical stimulus can promote neurite growth. Thus, neurite growth or cellular elongation may cause less compacting of chromatin, as suggested by a recent study showing that nuclear elongation correlates with neurite outgrowth and cellular elongation in this same neural cell line [27]. As such, the incidence of costimulus with these systems is undoubtedly a potential performance influencer and will be further investigated with transcriptome-, genome-, and epigenome-level studies.

As one understands genome-level changes due to ultrasonic and electrical costimulation, additional research can be done to identify comparative cell health markers. Electric and ultrasonic field computational models will be critical in understanding dose response of the system. One of the challenges and advantages of the highly attenuating ultrahighfrequency RF band is the localization spatially of the ultrasonic and electrical fields, as mentioned in the introduction. The highly localized ultrasonic field makes the design of the cell-transducer interface challenging compared with those at lower frequencies. At lower frequencies, due to low ultrasonic attenuation, the ultrasonic transducer interfaces with cell culture systems (multiwell plates, flasks, Petri dishes) through a water layer and is placed within a water bath. In this case, the culture container will act as an additional propagation medium for the ultrasonic wavefront [40], [41]. With highly attenuating ultrahigh-frequency US, this could

introduce additional energy dissipation and be much less similar to the biological interface used in potential medical and research applications. We aim to use an interface that directly couples with the cell culture medium and cells, within the attenuation length of the ultrahigh-frequency band. This constraint requires the control volume interface that places the cell culture approximately $10~\mu m$ from the chip interface.

Improvements to this interface include CMOS integration such that surface wire bonds in Device C do not interfere with the glass coverslip. While this study does not use surface functionalization to grow cells directly on the chip surface, this is an area for future investigation in addition to on-chip microfluidic chamber construction. Due to the initial evidence of poor growth of this cell line on silicon in addition to further attenuation introduced due to surface functionalization with collagen or fibronectin, cells were grown on a glass coverslip, inverted, and placed onto the silicon chip interface. The future vision to improve implementation of neural interfaces with these chips is toward CMOS and microfluidic integration, in addition to various US transducers of different frequencies. As this study uses ultrahigh frequency above 1 GHz to obtain theoretical lateral resolutions of 1 μ m with a reasonable axial localization, superhigh frequency presents with very steep axial localization. This could be of future interest with further transducer development, but to meet the single cell and subcellular localization desired in this and accompanying studies, ultrahigh band GHz regime resonance is chosen [1], [2]. With further process flow modifications and improvements, lower and higher resonance transducers may be introduced in the same chip, allowing for further evaluation of the influence of frequency modulation on the performance of the device and the downstream cellular bioeffects. Beam steering applications will allow for further resolution landmarks to be met.

V. CONCLUSION

GHz US and electrode chip-scale arrays for cells and tissueon-a-chip devices are promising next-generation technologies for tunable, ultrasonically activated electrodes. CMOS and microfluidics integration will refine device control toward these future directions. Further neuronal marker-specific staining, genome, transcriptome, and proteome analysis will be performed to conduct a detailed effect of GHz ultrasonic effects and electrical stimulation on neurons.

CONFLICT OF INTERESTS

Amit Lal is the founder of Geegah, which is commercializing the use of gigahertz (GHz) ultrasonic transducers.

ACKNOWLEDGMENT

Equipment and materials were previously purchased and used from the National Science Foundation and trusted integrated chips (TIC) Grant. The authors would like to thank the Institute of Microelectronics in Singapore (IME Singapore A*STAR) for fabrication of chips in collaboration with SonicMEMS Members as a part of the Intelligence Advanced Research Projects Activity (I-ARPA) TIC Program; they would also like to thank Dr. Edwin Kan for shared laboratory space and equipment; they also thank the resources, shared funding, and insights from Dr. Ankur Singh and Dr. Chris Xu; they also thank Kasra Kakavand, Jack Danieli, Eric Lawrence, and many others from the Applications Team at Polytec GmbH for arranging for equipment used to obtain displacement profiles of the gigahertz (GHz) transducer, performed at the Medically Advanced Devices Laboratory at the Center for Medical Devices in the Department of Mechanical and Aerospace Engineering, University of California San Diego. Thanks to the generous accommodations of Dr. James Friend, William Connacher, Ann Huang, Aditya Vasan, Eric Lawrence, Jiyang Mei, Shuai Zhang, and Naiqing Zhang. They also like to thank the generous accommodations of the Weill Cornell Microscopy and Image Analysis facility, specifically Dr. Sushmita Mukherjee and Lee Cohen-Gould for device images.

REFERENCES

- [1] P. S. Balasubramanian, A. Singh, C. Xu, and A. Lal, "GHz ultrasonic chip-scale device induces ion channel stimulation in human neural cells," *Sci. Rep.*, vol. 10, no. 1, pp. 1–20, Dec. 2020, doi: 10.1038/s41598-020-58133-0.
- [2] P. S. Balasubramanian and A. Lal, "Cellular localization and dosage regulation of neural stimulation enabled by 1.05 GHz ultrasonics," in *Proc. IEEE Int. Ultrason. Symp. (IUS)*, Oct. 2018, pp. 1–4, doi: 10.1109/ULTSYM.2018.8579899.
- [3] P. S. Balasubramanian, "Characterization of SH-SY5Y neurons subject to 92 kHz ultrasound stimulation," *Int. J. Morphol.*, vol. 39, no. 4, pp. 1109–1115, Aug. 2021, doi: 10.4067/S0717-95022021000401109.
- [4] V. Gilja, A. C. Chestek, I. Diester, J. M. Henderson, K. Deisseroth, and K. V. Shenoy, "Challenges and opportunities for next-generation intracortically based neural prostheses," *IEEE Trans. Biomed. Eng.*, vol. 58, no. 7, pp. 1891–1899, Jul. 2011, doi: 10.1109/TBME.2011.2107553.
- [5] R. B. Szlavik, "Strategies for improving neural signal detection using a neural-electronic interface," *IEEE Trans. Neural Syst. Rehabil. Eng.*, vol. 11, no. 1, pp. 1–8, Mar. 2003, doi: 10.1109/TNSRE.2003.810559.
- [6] Y. Tufail, A. Yoshihiro, S. Pati, M. M. Li, and W. J. Tyler, "Ultrasonic neuromodulation by brain stimulation with transcranial ultrasound," *Nature Protocols*, vol. 6, no. 9, pp. 1453–1470, 2011, doi: 10.1038/nprot.2011.371.
- [7] R. A. Green, N. H. Lovell, G. G. Wallace, and L. A. Poole-Warren, "Conducting polymers for neural interfaces: Challenges in developing an effective long-term implant," *Biomaterials*, vol. 29, nos. 24–25, pp. 3393–3399, 2008, doi: 10.1016/j.biomaterials.2008.04.047.
- [8] A. Bystritsky et al., "A review of low-intensity focused ultrasound pulsation," Brain Stimul., vol. 4, no. 3, pp. 125–136, Jul. 2011, doi: 10.1016/j.brs.2011.03.007.
- [9] H. Zheng, "Ultrasonic neuromodulation: Evidence from neuron to animal model," *Ultrasound Med. Biol.*, vol. 43, pp. S233–S234, Jan. 2017, doi: 10.1016/j.ultrasmedbio.2017.08.1816.

- [10] J. Kubanek, J. Shi, J. Marsh, D. Chen, C. Deng, and J. Cui, "Ultrasound modulates ion channel currents," Sci. Rep., vol. 6, no. 1, pp. 1–14, Apr. 2016, doi: 10.1038/srep24170.
- [11] W. Tang, Q. Liu, X. Wang, P. Wang, J. Zhang, and B. Cao, "Potential mechanism in sonodynamic therapy and focused ultrasound induced apoptosis in sarcoma 180 cells *in vitro*," *Ultrasonics*, vol. 49, no. 8, pp. 786–793, Dec. 2009, doi: 10.1016/j.ultras.2009.06.002.
- [12] I.-C. Lee, H.-J. Wu, and H.-L. Liu, "Dual-frequency ultrasound induces neural Stem/Progenitor cell differentiation and growth factor utilization by enhancing stable cavitation," ACS Chem. Neurosci., vol. 10, no. 3, pp. 1452–1461, Mar. 2019, doi: 10.1021/acschemneuro.8b00483.
- [13] Y. Lv, P. Zhao, G. Chen, Y. Sha, and L. Yang, "Effects of low-intensity pulsed ultrasound on cell viability, proliferation and neural differentiation of induced pluripotent stem cells-derived neural crest stem cells," *Biotechnol. Lett.*, vol. 35, no. 12, pp. 2201–2212, Dec. 2013, doi: 10.1007/s10529-013-1313-4.
- [14] I.-C. Lee et al., "Differentiation of neural stem/progenitor cells using low-intensity ultrasound," *Ultrasound Med. Biol.*, vol. 40, no. 9, pp. 2195–2206, Sep. 2014, doi: 10.1016/j.ultrasmedbio.2014.05.001.
- [15] Y. Feng, Z. Tian, and M. Wan, "Bioeffects of low-intensity ultrasound in vitro," J. Ultrasound Med., vol. 29, no. 6, pp. 963–974, Jun. 2010. [Online]. Available: http://www.jultrasoundmed.org/content/29/6/963.abstract
- [16] S. Noriega, G. Budhiraja, and A. Subramanian, "Remodeling of chromatin under low intensity diffuse ultrasound," *Int. J. Biochem. Cell Biol.*, vol. 44, no. 8, pp. 1331–1336, Aug. 2012, doi: 10.1016/j.biocel.2012.04.027.
- [17] W. Guo et al., "Self-powered electrical stimulation for enhancing neural differentiation of mesenchymal stem cells on graphene–poly(3,4-ethylenedioxythiophene) hybrid microfibers," ACS Nano, vol. 10, no. 5, pp. 5086–5095, May 2016, doi: 10.1021/acsnano.6b00200.
- [18] Y. Yang et al., "Facilitated neural differentiation of adipose tissue–derived stem cells by electrical stimulation and Nurr-1 gene transduction," Cell Transplantation, vol. 25, no. 6, pp. 1177–1191, Jun. 2016, doi: 10.3727/096368915x688957a.
- [19] T. Kondo *et al.*, "Hyperthermia with mild electrical stimulation protects pancreatic β-cells from cell stresses and apoptosis," *Diabetes*, vol. 61, no. 4, pp. 838–847, Apr. 2012, doi: 10.2337/db11-1098.
- [20] B. C. Thompson et al., "Conducting polymers, dual neurotrophins and pulsed electrical stimulation—Dramatic effects on neurite outgrowth," J. Controlled Release, vol. 141, no. 2, pp. 161–167, Jan. 2010, doi: 10.1016/j.jconrel.2009.09.016.
- [21] A. J. Evans et al., "Promoting neurite outgrowth from spiral ganglion neuron explants using polypyrrole/BDNF-coated electrodes," J. Biomed. Mater. Res. A, vol. 91A, no. 1, pp. 241–250, Oct. 2009, doi: 10.1002/jbm.a.32228.
- [22] L. Berdondini et al., "High-density electrode array for imaging in vitro electrophysiological activity," Biosensors Bioelectron., vol. 21, no. 1, pp. 167–174, Jul. 2005, doi: 10.1016/j.bios.2004.08.011.
- [23] A. Lal, "GHz ultrasonics for on chip delay lines, communications, timing, memory, and sensing," in *Proc. Joint Conf. Eur. Freq. Time Forum IEEE Int. Freq. Control Symp. (EFTF/IFC)*, Jul. 2017, p. 138, doi: 10.1109/FCS.2017.8088826.
- [24] E. M. Strohm, M. J. Moore, and M. C. Kolios, "High resolution ultrasound and photoacoustic imaging of single cells," *Photoacoustics*, vol. 4, no. 1, pp. 36–42, Mar. 2016, doi: 10.1016/j.pacs.2016.01.001.
- [25] S. Hu, C. Su, and W. Arnold, "Imaging of subsurface structures using atomic force acoustic microscopy at GHz frequencies," *J. Appl. Phys.*, vol. 109, no. 8, Apr. 2011, Art. no. 084324, doi: 10.1063/1.3573484.
- [26] M. M. Shipley, C. A. Mangold, and M. L. Szpara, "Differentiation of the SH-SY5Y human neuroblastoma cell line," *JoVE*, no. 108, pp. 1–11, Feb. 2016, doi: 10.3791/53193.
- [27] P. S. Balasubramanian, "Nuclear elongation correlates with neurite induced cellular elongation during differentiation of SH-SY5Y neural cells," *Int. J. Morphol.*, vol. 39, no. 2, pp. 548–553, Apr. 2021, doi: 10.4067/S0717-95022021000200548.
- [28] J. Prada, M. Sasi, C. Martin, S. Jablonka, T. Dandekar, and R. Blum, "An open source tool for automatic spatiotemporal assessment of calcium transients and local 'signal-close-to-noise' activity in calcium imaging data," *PLoS Comput. Biol.*, vol. 14, no. 3, Mar. 2018, Art. no. e1006054.
- [29] E. Picht, A. V. Zima, L. A. Blatter, and D. M. Bers, "Spark-Master: Automated calcium spark analysis with ImageJ," Amer. J. Physiol. Cell Physiol., vol. 293, no. 3, pp. 1073–1081, 2007, doi: 10.1152/ajpcell.00586.2006.

- [30] N. Tandon et al., "Alignment and elongation of human adipose-derived stem cells in response to direct-current electrical stimulation," in Proc. Annu. Int. Conf. IEEE Eng. Med. Biol. Soc., Sep. 2009, pp. 6517–6521, doi: 10.1109/IEMBS.2009.5333142.
- [31] I. A. Titushkin and M. R. Cho, "Controlling cellular biomechanics of human mesenchymal stem cells," in *Proc. Annu. Int. Conf. IEEE Eng. Med. Biol. Soc.*, Sep. 2009, pp. 2090–2093, doi: 10.1109/IEMBS.2009.5333949.
- [32] K. Kimura, Y. Yanagida, T. Haruyama, E. Kobatake, and M. Aizawa, "Gene expression in the electrically stimulated differentiation of PC12 cells," *J. Biotechnol.*, vol. 63, no. 1, pp. 55–65, 1998, doi: 10.1016/S0168-1656(98)00075-3.
- [33] F. Pires, Q. Ferreira, C. A. V. Rodrigues, J. Morgado, and F. C. Ferreira, "Neural stem cell differentiation by electrical stimulation using a cross-linked PEDOT substrate: Expanding the use of biocompatible conjugated conductive polymers for neural tissue engineering," *Biochimica et Biophysica Acta (BBA) Gen. Subjects*, vol. 1850, no. 6, pp. 1158–1168, Jun. 2015, doi: 10.1016/j.bbagen.2015.01.020.
- [34] K. L. Kilgore and N. Bhadra, "Reversible nerve conduction block using kilohertz frequency alternating current," *Neuromodulation, Tech*nol. *Neural Interface*, vol. 17, no. 3, pp. 242–254, Apr. 2014, doi: 10.1111/ner.12100.
- [35] R. Muratore, J. K. LaManna, M. R. Lamprecht, and B. Morrison III, "Hippocampal culture stimulus with 4-megahertz ultrasound," in *Proc. AIP Conf.*, 2012, pp. 254–258, doi: 10.1063/1.4757344.
- [36] E. Tomaskovic-Crook et al., "Human neural tissues from neural stem cells using conductive biogel and printed polymer microelectrode arrays for 3D electrical stimulation," Adv. Healthcare Mater., vol. 8, no. 15, Aug. 2019, Art. no. 1900425, doi: 10.1002/adhm.201900425.
- [37] C.-F.-V. Latchoumane *et al.*, "Chronic electrical stimulation promotes the excitability and plasticity of ESC-derived neurons following glutamate-induced inhibition *in vitro*," *Sci. Rep.*, vol. 8, no. 1, pp. 1–16, Dec. 2018, doi: 10.1038/s41598-018-29069-3.
- [38] Y.-J. Chang, C.-M. Hsu, C.-H. Lin, M. S.-C. Lu, and L. Chen, "Electrical stimulation promotes nerve growth factor-induced neurite outgrowth and signaling," *Biochimica Biophysica Acta (BBA) Gen. Subjects*, vol. 1830, no. 8, pp. 4130–4136, Aug. 2013, doi: 10.1016/j.bbagen.2013.04.007.
- [39] H. Ashush et al., "Apoptosis induction of human myeloid leukemic cells by ultrasound exposure," Cancer Res., vol. 60, no. 4, pp. 1014–1020, 2000.
- [40] K. Hensel, M. P. Mienkina, and G. Schmitz, "Analysis of ultrasound fields in cell culture wells for *in vitro* ultrasound therapy experiments," *Ultrasound Med. Biol.*, vol. 37, no. 12, pp. 2105–2115, Dec. 2011, doi: 10.1016/j.ultrasmedbio.2011.09.007.
- [41] W. Secomski, K. Bilmin, T. Kujawska, A. Nowicki, P. Grieb, and P. A. Lewin, "In vitro ultrasound experiments: Standing wave and multiple reflections influence on the outcome," *Ultrasonics*, vol. 77, pp. 203–213, May 2017, doi: 10.1016/j.ultras.2017.02.008.



Priya S. Balasubramanian received the B.S.E. degree in biomedical engineering from Duke University, Durham, NC, USA, in 2012, the M.S. degree in electrical engineering from Columbia University, New York City, NY, USA, in 2016, and the M.S. degree and Ph.D. degree in electrical and computer engineering from Cornell University, Ithaca, NY, USA, in 2020 and 2021, respectively.

She held a position with the Department of Radiology, Weill Cornell Medicine, New York City,

through the CU-WCGS Linkage Program. Her research interests include biodevices and MEMS, in particular neural interfaces. She has expertise in devices, cell biology, and computation with an emphasis in neuroscience field. Her dissertation research encompasses high-resolution neural engineering using localizable ultrasonic and electrical stimuli in

addition to computational algorithm development for the mapping of magnetic susceptibility distribution using magnetic resonance imaging data. She is interested in using human relevant models interfaced with computational and device-based techniques to further biology and biomedical science without the need to use animal models toward more ethical and conscientious scientific methodology.

Dr. Balasubramanian has received numerous awards, including the *Summa Cum Laude* and Graduation with Distinction honors at Duke University, the Tesla Scholarship and the National Science Foundation STEM SEGUE Fellowship for her M.S. degree at Columbia University, where she served as an Electrical Engineering Ambassador, the Cornell University Graduate Fellowship, the Cornell University Neurotechnology Fellowship, the Horizons Scholarship, the Kavli Institute TRF Scholarship, the ISMRM Educational Stipend, and the Ruth L. Kirschstein National Research Service Award from the National Institutes of Health (NIH) for Summer Clinical Immersion for her research at Cornell University. Her publications have won awards and been featured in major collections of various high-impact journals.



Amit Lal (Senior Member, IEEE) received the B.S. degree in electrical engineering from the California Institute of Technology, Pasadena, CA, USA, in 1990, and the Ph.D. degree in electrical engineering from the University of California at Berkeley, Berkeley, CA, USA, in 1996.

He was a Robert M. Scharf Professor with the School of Electrical and Computer Engineering, Cornell University, Ithaca, NY, USA, in 1977, where he directs the SonicMEMS Laboratory. His work has resulted in new fabrication and archi-

tectures in micro-/nano-electromechanical systems, physical acoustics, ultrasonics engineering, biomedical MEMS, microfluidics, analog and digital circuit design, solid-state electronics, radioactive thin films for autonomous microsystems, and nanofabrication. He is an Evangelist for teaching through "Holy Grails" of future technology. From 2005 to 2009, he served as a Program Manager with the Microsystems Technology Office, Defense Advanced Research Projects Agency, Arlington, VA, USA, where he developed and managed programs in the areas of navigation, low-energy computation, bio-robotics, and atomic microsystems. He has been awarded 33 patents and published more than 185 research articles in the area of microsystem engineering. His technical interests and activities are focused on developing new technologies.

Dr. Lal was a recipient of the NSF CAREER, the Whitaker Foundation Award, the Department of Defense Exceptional Service Award, and the Best Program Manager Award. With his students, he has been awarded several best paper awards at the IEEE Ultrasonics Symposium and MEMS Conferences.